Dynamic response of a monorail steel bridge under a moving train

Lee, Chang Hun
Kawatani, Mitsuo
Kim, Chul Woo
Nishimura, Nobuo
Kobayashi, Y.

(Citation)
Journal of Sound and Vibration,294(3):562-579

(Issue Date)
2006-06

(Resource Type)
journal article

(Version)
Accepted Manuscript

(URL)
https://hdl.handle.net/20.500.14094/90000160

Dynamic Response of a Monorail Steel Bridge under a Moving Train

C. H. LEE,
M. of Eng., Graduate School of Engineering, Osaka University, 2-1 Yamadaoka, Suita, Osaka 565-0871, Japan
*M. KAWATANI,
Dr. of Eng., Prof., Dept. of Civil Eng., Kobe University, 1-1 Rokkodai, Nada, Kobe 657-8501, Japan
Fax: +81-78-803-6069. *E-mail address* : m-kawa@kobe-u.ac.jp
C. W. KIM,
Ph.D., Dept. of Civil Eng., Kobe University, 1-1 Rokkodai, Nada, Kobe 657-8501, Japan
N. NISHIMURA
Dr. of Eng., Prof., Dept. of Civil Eng., Osaka University, 2-1 Yamadaoka, Suita, Osaka 565-0871, Japan
AND
Y. KOBAYASHI
Dr. of Eng., Steel Structures & Ocean Laboratory, Technical Research Institute, Hitachi Zosen Co., 2-2-11 Funamachi, Taisho, Osaka 551-0022, Japan

This study proposes a dynamic response analysis procedure for traffic-induced vibration of a monorail bridge and train. Each car in the monorail train is idealized as a dynamic system of 15-degrees-of-freedom. The governing equations of motion for a three-dimensional monorail bridge-train interaction system are derived using Lagrange's formulation for monorail trains, and a finite element method for modal analysis of monorail bridges. Analytical results on dynamic response of the monorail train and bridge are compared with field-test data in order to verify the validity of the proposed analysis procedure, and a positive correlation is found. An interesting feature of the monorail bridge response is that sway motion is caused by torsional behavior resulting from eccentricity between the shear center of the bridge section and the train load.

Key Words: Monorail bridge, Monorail-train, Field test, Dynamic response analysis, 15DOF of train model, Traffic-induced vibration analysis

1. INTRODUCTION

In the last two decades, there has been a significant need for new transportation systems due to traffic problems in major cities of the world, including Japan. This need to adopt new transportation systems has produced the monorail systems in Tokyo, Osaka, Tama, Kita-Kyusyu, and Naha of Japan.

In contrast with railway bridges, a monorail system employs steering and stabilizing wheels to firmly grasp the track girder of monorail bridges and, as a result, the rolling of monorail trains can affect the dynamic response of the bridge. A few three-dimensional analytical models of the bridge-car interaction system have been developed for highway (for example, [1-4]) and railway bridges [5-10]. Some studies have even focused on the vibration of a railway track under moving trains. Xia *et al.* [8] studied the dynamic interaction of long suspension bridges with running trains, and a three-dimensional finite element model was used to represent the long suspension bridge. Lei *et al.* [9] developed a dynamic computational model for the car and track coupling system using the finite element method. Ju *et al.* [10] studied the vibration characteristics of a three-dimensional arch bridge under the running of high-speed trains. However, little useful data on the dynamic response of monorail trains and bridges has been reported as yet.

This study proposes a dynamic response analysis procedure for traffic-induced vibration of a monorail bridge and train. The governing equations of the monorail bridge-train interaction system are derived using Lagrange's formulation for monorail trains, taking the surface roughness into account, and using the finite element method for modal analysis of the monorail bridge. The validity of the proposed analysis procedure for traffic-induced vibration of monorail bridges is verified by comparison with field-test data for the monorail system. Field measurement was carried out during operation. The surface roughness of track girders was measured, and used in the analysis. Analytical results on the displacement and acceleration of the monorail bridge and the acceleration of a car in the monorail train were compared with field-test data.

2. THEORETICAL PROCEDURE FOR MONORAIL TRAIN-BRIDGE INTERACTION

2.1 Bridge system

The typical configuration of the Osaka monorail steel structure is shown in Figure 1. The structure consists of two steel box track girders, cross beams, lateral bracings, supports and piers. The finite element (FE) method for modal analysis is used as a tool for idealizing bridges for dynamic response analysis [11]. Bridges are considered to be an assemblage of beam elements with six-degrees-of-freedom at each node. The consistent mass system and Rayleigh damping [12] are used, respectively, to form the mass and damping matrices of the bridge model. A process known as Guyan reduction is used to improve the efficiency of calculation [13].

The equation for forced vibration of a bridge system under a moving monorail train is given in Eq. (1):

$$\mathbf{M_b}\ddot{\mathbf{w}}_\mathbf{b} + \mathbf{C_b}\dot{\mathbf{w}}_\mathbf{b} + \mathbf{K_b}\mathbf{w_b} = \mathbf{f}_b \tag{1}$$

where, $\boldsymbol{M_b}$, $\boldsymbol{C_b}$, and $\boldsymbol{K_b}$ respectively denote the mass, damping and stiffness matrices of the bridge. $\boldsymbol{w}_b$ indicates the displacement vector of the bridge. $\boldsymbol{f_b}$ is an external force vector due to the moving monorail train. $(\cdot)$ represents the derivative with respect to time.

Rayleigh damping gives the damping matrix $\boldsymbol{C}_b$, based on the assumption that it is a linear combination of the mass and stiffness matrices [12] as shown in Eq. (2):

$$\mathbf{C_b} = p\mathbf{M_b} + q\mathbf{K_b} \tag{2}$$

where, p and q are constants, obtained by solving the two simultaneous equations which result upon specifying the damping ratio for two modes of vibration [12]. Using the first two modes the constants are as follows:

$$p = \frac{2\omega_1\omega_2\left(h_1\omega_2 - h_2\omega_1\right)}{\omega_2^2 - \omega_1^2} \tag{3}$$

$$q = \frac{2\left(h_2\omega_2 - h_1\omega_1\right)}{\omega_2^2 - \omega_1^2} \tag{4}$$

where, ω and h are the angular frequency and damping ratio, respectively. The values of the damping ratio for higher modes can then be determined by:

$$h_i = \frac{p + q\omega_i^2}{2\omega_i} \tag{5}$$

The displacement vector of the bridge $\boldsymbol{w_b}$ can be defined in terms of the normal coordinates q_i and mode vector ϕ_i as follows:

$$\mathbf{w}_b = \sum_i \phi_i q_i = \mathbf{\Phi} \cdot \mathbf{q} \tag{6}$$

2.2 Monorail train

A monorail car has two bogies which are each composed of pneumatic tires for running/steering and stabilizing wheels. A photograph of the monorail train is shown in Figure 2. The dynamic behavior of the car is assumed to be sufficiently represented by a discrete rigid multi-body system with 15-degrees-of-freedom (DOF) as shown in Figure 3, where $\boldsymbol{m}$ indicates the mass; $\boldsymbol{K}$, the spring constant; $\boldsymbol{C}$, the damping coefficient; and $\boldsymbol{z}$, $\boldsymbol{y}$ and $\boldsymbol{\theta}$ indicate, respectively, the vertical, lateral and rotational displacement. The sign is positive if the direction of deformation is downward. Pitching occurs from the rear bogie to the front bogie, rolling from the right side to the left side and the yawing from the front to the rear.

Governing equations for a car in the monorail train are derived using an energy method based on the Lagrange equation of motion, as shown in Eq. (7). This is one of the most popular methods for formulating a dynamic system with great power and diverse utility [14, 15].

$$\frac{\partial}{\partial t}\left(\frac{\partial T}{\partial \dot{a}_i}\right) - \frac{\partial T}{\partial a_i} + \frac{\partial U_e}{\partial a_i} + \frac{\partial U_d}{\partial \dot{a}_i} = 0 \tag{7}$$

where, T is the kinetic energy, U_e is the potential energy, U_d is the dissipation energy of the system, and a_i is a generalized coordinate.

The kinetic energy, potential energy and dissipation energy of a train on a bridge are developed by modifying the energy equation for a vehicle on a highway bridge [16, 17]. These energy equations are expressed in a set of generalized coordinates as follows:

$$\begin{aligned} T = \frac{1}{2}\sum_{v=1}^{nv}\Big[& m_{v11}\dot{Z}_{v11}^{\,2} + m_{v11}\dot{Y}_{v11}^{\,2} + I_{vx11}\dot{\theta}_{vx11}^{\,2} + I_{vy11}\dot{\theta}_{vy11}^{\,2} + I_{vz11}\dot{\theta}_{vz11}^{\,2} \\ & + \sum_{i=1}^{2}\left\{ m_{v2i}\dot{Z}_{v2i}^{\,2} + m_{v2i}\dot{Y}_{v2i}^{\,2} + I_{vx2i}\dot{\theta}_{vx2i}^{\,2} + I_{vy2i}\dot{\theta}_{vy2i}^{\,2} + I_{vz2i}\dot{\theta}_{vz2i}^{\,2} \right\} \Big] \end{aligned} \tag{8}$$

$$U_e = \tfrac{1}{2}\sum_{v=1}^{nv}\left[\sum_{i=1}^{2}\sum_{j=1}^{2}\sum_{n=1}^{2}\left\{ K_{vi1jn}R_{vi1jn}^{\,2}\delta_{1j} + K_{vi2jn}R_{vi2jn}^{\,2} + K_{vi3jn}R_{vi3jn}^{\,2} + K_{vi4jn}R_{vi4jn}^{\,2}\delta_{1j} \right\} + \sum_{i=1}^{2} K_{vi511}R_{vi511}^{\,2} \right] \tag{9}$$

$$U_d = \tfrac{1}{2}\sum_{v=1}^{nv}\left[\sum_{i=1}^{2}\sum_{j=1}^{2}\sum_{n=1}^{2}\left\{ C_{vi1jn}\dot{R}_{vi1jn}^{\,2}\delta_{1j} + C_{vi2jn}\dot{R}_{vi2jn}^{\,2} + C_{vi3jn}\dot{R}_{vi3jn}^{\,2} + C_{vi4jn}\dot{R}_{vi4jn}^{\,2}\delta_{1j} \right\} + \sum_{i=1}^{2} C_{vi511}\dot{R}_{vi511}^{\,2} \right] \tag{10}$$

where, *nv* is the number of cars in a monorail train, *I* is the mass moment of inertia, the subscript v is the number of cars on the bridge, the subscript *i* is an index indicating the suspension position of a car (*i*=1 and 2 are the front and rear suspensions, respectively), the subscript *j* is the tire position in a bogie (*j*=1 and 2 are the front and rear tires of the bogie system, respectively), *n* is an index indicating the left and right sides of the car, and R_{vimjn} is the relative displacement at springs/dampers. δ_{ij} is Kronecker's delta. Details of the notation are summarized in Table 1.

Relative displacement can be defined as follows:

$$R_{vi1\,jn} = Z_{v11} - Z_{v2i} + (-1)^n \theta_{vx11} L_{vy2} - (-1)^n \theta_{vx2i} L_{vy2} - (-1)^i \theta_{vy11} L_{vxi} \tag{11}$$

$$R_{vi2\,jn} = Z_{v2i} - (-1)^j \theta_{vy2i} L_{vx3} + (-1)^n \theta_{vx2i} L_{vy4} - V_{0i2\,jn} \tag{12}$$

$$R_{vi3\,jn} = Y_{v2i} - V_{0i3\,jn} + (-1)^j \theta_{vz2i} L_{vx4} \tag{13}$$

$$R_{vi4\,jn} = Y_{v2i} - V_{0i4\,jn} + \theta_{vx2i} L_{vz3} \tag{14}$$

$$R_{vi5\,jn} = Y_{v11} - Y_{v2i} - \theta_{vx11} L_{vz1} + (-1)^i \theta_{vz11} L_{vxi} \tag{15}$$

where, V_{0imjn} denotes the relative displacement of the bridge and surface roughness at the contact points of wheel positions. Appendix A gives details on the governing equation for a car in a monorail train.

2.3 Monorail bridge- train interaction

The load vector due to a moving monorail train is given by Eq. (16).

$$\mathbf{f}_b = \sum_{v=1}^{nv} \sum_{i=1}^{2} \sum_{m=1}^{5} \sum_{j=1}^{2} \sum_{n=1}^{2} \boldsymbol{\Psi}_{vimjn}(t) \mathbf{P}_{vimjn}(t) \tag{16}$$

where, $\boldsymbol{\Psi}_{vimjn}(t)$ is the distribution vector which distributes wheel loads through a beam element to each node of the element, and $\mathbf{P}_{vimjn}(t)$ is the wheel load of the monorail train. The wheel loads, such as the lateral forces at the steering and stabilizing wheels and the vertical force at the driving wheels, are expressed, respectively, by Eqs. (17) and (18) as indicated below:

$$P_y = \begin{cases} P_{vi3\,jn} = K_{vi3\,jn} R_{vi3\,jn} + C_{vi3\,jn} \dot{R}_{vi3\,jn} & (\textit{Steering-wheel}) \\ P_{vi41n} = K_{vi41n} R_{vi41n} + C_{vi41n} \dot{R}_{vi41n} & (\textit{Stabilizing-wheel}) \end{cases} \tag{17}$$

$$P_z = P_{vi2\,jn} = \frac{1}{4} \left\{ m_{v11} g \left(1 - \frac{L_{vxi}}{L_{vx}} \right) + m_{v2i} g \right\} + K_{vi2\,jn} R_{vi2\,jn} + C_{vi2\,jn} \dot{R}_{vi2\,jn} \tag{18}$$

where, m_{v11}, m_{v21} and m_{v22} indicate, respectively, the concentrated mass of the train's body, and the front and rear bogies. *g* denotes gravitational acceleration. K_{vimjn} and C_{vimjn} are the spring constant and damping coefficient of cars in the monorail train.

The simplified matrix form of the monorail bridge-train interaction can be expressed as follows.

$$\begin{bmatrix} \mathbf{M}_b & 0 \\ Symm. & \mathbf{M}_v \end{bmatrix} \begin{Bmatrix} \ddot{q} \\ \ddot{\Delta} \end{Bmatrix} + \begin{bmatrix} \mathbf{C}_b^{*} & \mathbf{C}_{bv} \\ Symm. & \mathbf{C}_v \end{bmatrix} \begin{Bmatrix} \dot{q} \\ \dot{\Delta} \end{Bmatrix} + \begin{bmatrix} \mathbf{K}_b^{*} & \mathbf{K}_{bv} \\ Symm. & \mathbf{K}_v \end{bmatrix} \begin{Bmatrix} q \\ \Delta \end{Bmatrix} = \begin{Bmatrix} \mathbf{f}_b \\ \mathbf{f}_v \end{Bmatrix} \tag{19}$$

where, $\mathbf{M}_b$ and $\mathbf{M}_v$ represent, respectively, the mass matrices of the monorail bridge and train. $\mathbf{C}_b^{*}$, $\mathbf{C}_v$ and $\mathbf{C}_{bv}$ represent the damping matrices of the monorail bridge, train and bridge-train interaction system, while $\mathbf{K}_b^{*}$, $\mathbf{K}_v$ and $\mathbf{K}_{bv}$ indicate the stiffness matrices for the same system.

2.4 Numerical algorithm

The dynamic equation for the monorail bridge-train interaction is a non-stationary dynamic problem since the coefficient matrices of the equations vary over time. Thus, the simultaneous differential equations involved in the bridge-train interaction system are solved using Newmark's β method as the numerical integration technique [18]. β of 0.25 is used to obtain stable and accurate solutions. Solutions can be obtained with a relative margin of error of less then 0.001. Figure 4 shows the algorithm for analyzing monorail bridge-train interaction. Dynamic response of the bridge is estimated by superposing up to the 50th mode (f_{50}=131.27 Hz). One fifth of the highest natural period is used as the time interval (Δt) in the analysis.

3. FIELD-TEST

To verify the validity of the monorail train-bridge interaction analysis developed here, a monorail steel bridge with a span of 34.8 m (see Figure 5) was tested and analyzed under a moving train. The acceleration and displacement response of the bridge were measured in a field-test. On the train side, the acceleration response of the second car in the monorail train was recorded. The test involved surveying the surface roughness of the tracks.

3.1 Monorail steel bridge

Figure 5 and Table 2 show, respectively, the configuration and structural properties of the tested bridge. A digital video camera equipped with a telescope was used to measure the dynamic displacement of the bridge. Image processing was used to convert the recorded image to displacements. Accelerometers and displacement measurement targets were positioned at the span center of the bridge as shown in Figure 6.

3.2 Monorail train

To examine the dynamic responses of a monorail train, accelerometers for the vertical and lateral directions were installed at a position 1.45 m to the left of, and 2.05 m back from the front axle of the second car in the train (see Figure 7). The properties of the empty train used in this test are summarized in Table 3. Passenger numbers were counted during the test as summarized in Table 4. The average traveling speed of the monorail train is recorded to be about 55 km/h, and this is used in the analysis for comparison with experiments. For initial condition of the monorail train when the trains entered a bridge, running monorail trains are already in a vibration state due to surface roughness before entering the bridge in the analysis. The mass of the train in the analysis is decided as with passenger numbers counted during the test.

3.3 Surface roughness

The field-test involved profiling the surface roughness of tracks for use in dynamic response analysis. Figure 8 shows the positions measured. An electronic staff and laser level (TX-22: E-base Co., Ltd., Japan) were used to measure the surface roughness (see Figure 9). The electronic staff and laser level were installed, respectively, at the inspection car and the end of the span. A high-pass filtering technique was used to truncate the static component due to the weight of the inspection car during profiling. The power spectral density curves of the measured profiles were plotted with ISO estimates [19] (see Figure 10) to assess the condition of the roughness and to generate artificial surface profiles. The bold line in Figure 10 indicates the measured PSD curve. Equation (20) provides the equation for curve fitting [20].

$$S_{z0}(\Omega) = \frac{\alpha}{\Omega^{n} + \beta^{n}} \tag{20}$$

where, $S_{z0}(\Omega)$ is the power spectral density of the surface roughness; Ω is the spatial frequency (cycle/m); and α, β and n are, respectively, the roughness coefficient, shape parameter and a parameter to express the distribution of power of a given PSD curve[20].

The parameters of Eq. (20) are assumed as the following based on measurements of a monorail bridge. For information, Figure 11 shows the artificial surface profile taken from a Monte-Carlo simulation method and measurement, in which the measurement was carried out for an observed bridge with span of 36 m long. The parameters in Eq. (20) are estimated to be:

Riding track : α= 0.0005, β= 0.35, n = 3.00
Steering-guideway : α= 0.0006, β= 0.5, n = 2.80
Stabilizing-guideway : α= 0.0006, β= 0.5, n = 2.60

4. NUMERICAL RESULTS

4.1 Eigen value analysis of bridge and trains

Table 5 shows the mode shapes and natural frequencies of the observation bridge derived from eigen value analysis. The first mode shows that vibration of the monorail bridge is dominated by a lateral bending mode. For the monorail train, the sway motion of the body has the lowest natural frequency as listed in Table 6. Observations also indicate that the difference in frequency between the lateral modes (2.806 Hz) of the bridge and car (0.912 Hz) ensures little possibility of resonance between two systems.

4.2 Comparison of analytical results with field measurements

Comparison of analytical results with field-test data is summarized in Figures 12, 13 and 14. Figure 12 shows the dynamic displacement response to the moving train in the vertical and lateral directions at the span center of the track girder, obtained from analysis and field-tests. Analysis yields displacements of 11.8 mm and 1.33 mm in the vertical and lateral directions, respectively. The corresponding values for vertical and lateral displacement from the field test were 11.5 mm and 1.05 mm, respectively. This shows that the analytic values agree well with field test results. The lateral displacement of the monorail bridge is caused by a torsional effect due to the eccentricity between the shear center of the bridge and the vertical load of the train.

It is noteworthy that, in bridge modeling, no special calibration was carried out but the existing drawings and design reports are used.

On the other hand, for modeling the train, the properties provided by the monorail train manufacturer were used. In comparing the analytical result with measured ones, the artificial surface profile showing the best agreement among 100 samples with the measured profiles as shown in Figure 11 is used in the analysis.

The acceleration responses at the observation point of the bridge and the second car in the monorail train, found by analysis and field-testing of the bridge, are shown in Figures 13 and 14. Figure 13 shows that the amplitude of the field-test acceleration in the vertical and lateral directions is slightly greater than that predicted by analysis. The Fourier spectrum shows that the dominant frequencies in field-tests and analysis are located, respectively, near 5.267 Hz and 5.096 Hz relative to the vertical and lateral bending modes (see Table 5).

Figure 14 shows the analytical and experimental acceleration responses of the monorail train. The analytical results for acceleration responses of the car in both the lateral and vertical directions also agree well with field test results, even though the hinge between the cars is neglected in modeling the monorail train. As for the spectrum, experimental results on the dominant frequency are observed to have a smaller set of values than those given by analysis. It is noteworthy that the load effect of the passengers counted during the field-test is regarded, in analysis, as 60 kg of mass per passenger.

It is a natural consequence that the actual phenomena of the monorail bridge-train interaction system are expressed well by the proposed analytical method, because the time history profile and Fourier spectrum of the theoretical response match well with those obtained in experimental results, in the light of potential sources of error. However, measured results have significant additional peaks in the amplitude of acceleration frequency domain compared with the analytic ones. One of the reasons for the phenomenon may be the difference of the train model compared with the real one; that is, the effect of motor, mechanical system, and others of the real train on experimental results may provide the difference. Another reason for the phenomenon may be the difference of surface profiles used in analysis compared with those of experiment even though the most similar surface profile among the simulated profile samples is used in the analysis.

5. CONCLUSION

A procedure was proposed for analyzing traffic-induced vibration of a monorail bridge under a moving monorail train. The analytical displacement and acceleration at the span center of the bridge were compared with field-test results in order to verify the validity of the procedure. The effectiveness of an analytical method for dynamic response of the train was also investigated by comparing with experiment. The major conclusions that can be drawn from this study are as follows:

1) The natural frequency difference between the lateral modes of the bridge (2.806 Hz) and car (0.912Hz) ensures little possibility of resonance between the two systems.
2) The dynamic displacement found by analysis agrees well with field test results. It is noteworthy that the lateral displacement of the monorail bridge is caused by a torsional effect due to the eccentricity between the shear center of the bridge and the vertical load of the trains.
3) The acceleration response in the vertical and lateral directions, found by analysis, also matches reasonably well with field-test

results.

4) The experimental results for acceleration response of the car in both lateral and vertical directions agree well with field test results, even though the hinge between the cars is neglected in modeling the monorail train.
5) The validity of the proposed analytical procedure suggests that it can be used for further study, in areas such as riding comfort of the train, and seismic response analysis of the monorail bridge-train interaction system.

ACKNOWLEDGEMENTS

The authors wish to acknowledge the assistance given to them by Osaka Monorail Co., LTD. Thanks also go to a former graduate student Mr. Kamizono of Kyobashi Mentech Co., LTD, Mr. Kanbara, a graduate student of Osaka University and Mr. Phimmasone, a graduate student of Kobe University for their kind support.

APPENDIX A.

EQUATION OF MOTION OF A CAR WITH 15DOF IN A MONORAIL TRAIN

The equation of motion for a car in a monorail train can be derived by substituting equations (7), (8) and (9) into Eq. (6) as follows:

Z_{v11}: Bouncing

$$m_{v11}\ddot{Z}_{v11} + \sum_{i=1}^{2}\sum_{j=1}^{2}\sum_{n=1}^{2}\left\{K_{vi1jn}R_{vi1jn} + C_{vi1jn}\dot{R}_{vi1jn}\right\}\delta_{1j} = 0 \tag{A.1}$$

Z_{v21}: Axle hop (Front-bogie)

$$m_{v21}\ddot{Z}_{v21} + \sum_{j=1}^{2}\sum_{n=1}^{2}\left\{-K_{v11jn}R_{v11jn}\delta_{1j} + K_{v12jn}R_{v12jn} - C_{v11jn}\dot{R}_{v11jn}\delta_{1j} + C_{v12jn}\dot{R}_{v12jn}\right\} = 0 \tag{A.2}$$

Z_{v22}: Axle hop (Rear-bogie)

$$m_{v22}\ddot{Z}_{v22} + \sum_{j=1}^{2}\sum_{n=1}^{2}\left\{-K_{v21jn}R_{v21jn}\delta_{1j} + K_{v22jn}R_{v22jn} - C_{v21jn}\dot{R}_{v21jn}\delta_{1j} + C_{v22jn}\dot{R}_{v22jn}\right\} = 0 \tag{A.3}$$

Y_{v11}: Lateral translation

$$m_{v11}\ddot{y}_{v11} + \sum_{i=1}^{2}\left\{K_{vi511}R_{vi511} + C_{vi511}\dot{R}_{vi511}\right\} = 0 \tag{A.4}$$

Y_{v21}: Bogie sway (Front-bogie)

$$\begin{aligned} m_{v21}\ddot{y}_{v21} + \sum_{j=1}^{2}\sum_{n=1}^{2}\left\{K_{v13jn}R_{v13jn} + C_{v13jn}\dot{R}_{v13jn} + K_{v14jn}R_{v14jn}\delta_{1j} + C_{v14jn}\dot{R}_{v14jn}\delta_{1j}\right\} \\ - K_{v1511}R_{v1511} - C_{v1511}\dot{R}_{v1511} = 0 \end{aligned} \tag{A.5}$$

Y_{v22}: Bogie sway (Rear-bogie)

$$\begin{aligned} m_{v22}\ddot{y}_{v22} + \sum_{j=1}^{2}\sum_{n=1}^{2}\left\{K_{v23jn}R_{v23jn} + C_{v23jn}\dot{R}_{v23jn} + K_{v24jn}R_{v24jn}\delta_{1j} + C_{v24jn}\dot{R}_{v24jn}\delta_{1j}\right\} \\ - K_{v2511}R_{v2511} - C_{v2511}\dot{R}_{v2511} = 0 \end{aligned} \tag{A.6}$$

θ_{vx11}: Rolling

$$I_{vx11}\ddot{\theta}_{vx11} + \sum_{i=1}^{2}\Big[\sum_{n=1}^{2}\Big\{(-1)^n L_{vy2}\left(K_{vi11n}R_{vi11n} + C_{vi11n}\dot{R}_{vi11n}\right)\Big\} + L_{vz1}\left(K_{vi51n}R_{vi51n} + C_{vi51n}\dot{R}_{vi51n}\right) - m_{v11}g\theta_{vx11}L_{vz2i}\Big] = 0 \tag{A.7}$$

θ_{vx21}: Axle tramp (Front-bogie)

$$I_{vx21}\ddot{\theta}_{vx21} + \sum_{j=1}^{2}\sum_{n=1}^{2}\Big[-(-1)^n L_{vy2}\left\{K_{v11jn}R_{v11jn} + C_{v11jn}\dot{R}_{v11jn}\right\}\delta_{1j} + (-1)^n L_{vy4}\left\{K_{v12jn}R_{v12jn} + C_{v12jn}\dot{R}_{v12jn}\right\} + L_{vz3}\left\{K_{v14jn}R_{v14jn} + C_{v14jn}\dot{R}_{v14jn}\right\}\delta_{1j}\Big] = 0 \tag{A.8}$$

θ_{vx22}: Axle tramp (Rear-bogie)

$$I_{vx22}\ddot{\theta}_{vx22} + \sum_{j=1}^{2}\sum_{n=1}^{2}\Big[-(-1)^n L_{vy2}\left\{K_{v21jn}R_{v21jn} + C_{v21jn}\dot{R}_{v21jn}\right\}\delta_{1j} + (-1)^n L_{vy4}\left\{K_{v22jn}R_{v22jn} + C_{v22jn}\dot{R}_{v22jn}\right\} + L_{vz3}\left\{K_{v24jn}R_{v24jn} + C_{v24jn}\dot{R}_{v24jn}\right\}\delta_{1j}\Big] = 0 \tag{A.9}$$

θ_{vy11}: Pitching

$$I_{vy11}\ddot{\theta}_{vy11} + \sum_{i=1}^{2}\sum_{n=1}^{2}\Big\{-(-1)^i L_{vxi}\left(K_{vi11n}R_{vi11n} + C_{vi11n}\dot{R}_{vi11n}\right)\Big\} = 0 \tag{A.10}$$

θ_{vy21}: Bogie Windup（Front-bogie）

$$I_{vy21}\ddot{\theta}_{vy21} - \sum_{j=1}^{2}\sum_{n=1}^{2}(-1)^j L_{vx3}\left\{K_{v12jn}R_{v12jn} + C_{v12jn}\dot{R}_{v12jn}\right\} = 0 \tag{A.11}$$

θ_{vy22}: Bogie Windup（Rear-bogie）

$$I_{vy22}\ddot{\theta}_{vy22} - \sum_{j=1}^{2}\sum_{n=1}^{2}(-1)^j L_{vx4}\left\{K_{v22jn}R_{v22jn} + C_{v22jn}\dot{R}_{v22jn}\right\} = 0 \tag{A.12}$$

θ_{vz11}: Yawing

$$I_{vz11}\ddot{\theta}_{vz11} + \sum_{i=1}^{2}(-1)^i L_{vxi}\left\{K_{vi511}R_{vi511} + C_{vi511}\dot{R}_{vi511}\right\} = 0 \tag{A.13}$$

θ_{vz21}: Bogie yawing (Front-bogie)

$$I_{vz21}\ddot{\theta}_{vz21} + \sum_{j=1}^{2}\sum_{n=1}^{2}\Big[(-1)^j L_{vx4}\left\{K_{v13jn}R_{v13jn} + C_{v13jn}\dot{R}_{v13jn}\right\}\Big] = 0 \tag{A.14}$$

θ_{vz22}: Bogie yawing (Rear-bogie)

$$I_{vz22}\ddot{\theta}_{vz22} + \sum_{j=1}^{2}\sum_{n=1}^{2}\Big[(-1)^j L_{vx4}\left\{K_{v23jn}R_{v23jn} + C_{v23jn}\dot{R}_{v23jn}\right\}\Big] = 0 \tag{A.15}$$

REFERENCES

[1] S.G. Hutton, Y.K. Cheung, Dynamic response of single span highway bridges. *Earthquake Engineering and Structural Dynamics* 7 (1979) 543-553.

[2] N.L. Mulcathy, Bridge response with tractor-trailer vehicle loading. *Earthquake Engineering and Structural Dynamics* 11 (1983) 649-665.

[3] J.W. Kou, J.T. DeWolf, Vibrational behavior of continuous span highway bridge-Influencing variables. *Journal of Structural*

Engineering, ASCE 123 (1997) 333-344.
[4] D. Huang, T.L. Wang, Vibration of highway steel bridges with longitudinal grades. *Computers and Structures* 69 (1998) 235-245.
[5] K. Ono, M. Yamada, Analysis of railway track vibration. *Journal of Sound and Vibration* 130 (1989) 269-297.
[6] L. Fryba, Dynamics of railway bridges, 2nd ed., Thomas Telford, London, 1996.
[7] J.D. Yau, Y.B. Yang, S.R. Kuo, Impact response of high speed rail bridges and riding comfort of rail cars. *Engineering Structures* 21 (1999) 836-844.
[8] H. Xia, Y.L. Xu, T.H.T. Chan, Dynamic interaction of long suspension bridges with running trains. *Journal of Sound and Vibration* 237 (2000) 263-280.
[9] X. Lei, N.A. Noda, Analyses of dynamic response of vehicle and track coupling system with random irregularity of track vertical profile. *Journal of Sound and Vibration* 258 (2002) 147-165.
[10] S.H. Ju, H.T. Lin, Numerical investigation of a steel arch bridge and interaction with high-speed trains. *Engineering Structures* 25 (2003) 241-250.
[11] K.J. Bathe, Finite element procedure in engineering analysis, Prentice-Hall, Englewood Cliffs, 1982
[12] M.E. Agabein, The effect of various damping assumptions on the dynamic response of structures. *Bulletin of International Institute of Seismology and Earthquake Engineering* 8 (1971) 217-236.
[13] R.J. Guyan, Reduction of stiffness and mass matrices. *AIAA Journal* 3 (2) (1965) 380.
[14] W.C. Hurty, M.F. Rubinstein, Dynamics of structures. Prentice-Hall, Englewood Cliffs, 1960, pp. 90-103.
[15] W.T. Thomson, Theory of Vibration with Applications. Prentice-Hall, Englewood Cliffs, 1988, pp. 196-198.
[16] M. Kawatani, C.W. Kim, Computer simulation for dynamic wheel loads of heavy trains. *Structural Engineering and Mechanics* 12 (2001) 409-428.
[17] C.W. Kim, M. Kawatani, K.B. Kim, Three-dimensional dynamic analysis for bridge-vehicle interaction with roadway roughness. *Computers & Structures* 83 (2005) 1627-1645.
[18] N.M. Newmark, A Method of computation for structural dynamics. *American Society of Civil Engineers, Journal of Engineering Mechanics Division* 85(EM3) (1970) 67-94.
[19] International Organization for Standardization ISO 8608, Mechanical Vibration - Road Surface Profiles - Reporting of Measured Data, 1995.
[20] H. Honda, Y. Kajikawa, T. Kobori, Spectra of road surface roughness on bridges. *American Society of Civil Engineers, Journal of Structural Division* 108 (2) (1982) 1956-1966.

Figure 1. View of the monorail steel bridge.

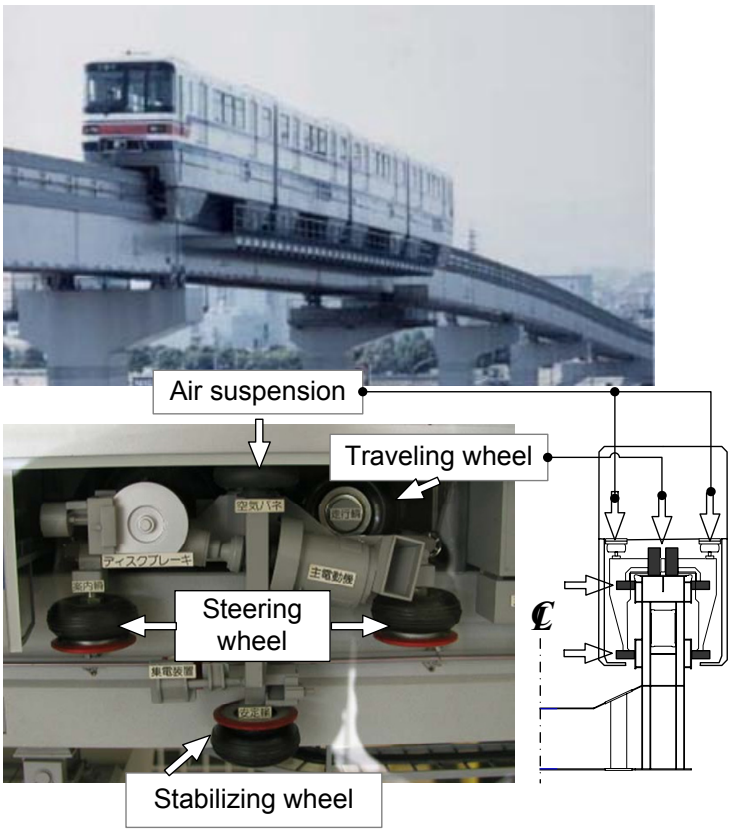

Figure 2. Monorail-train

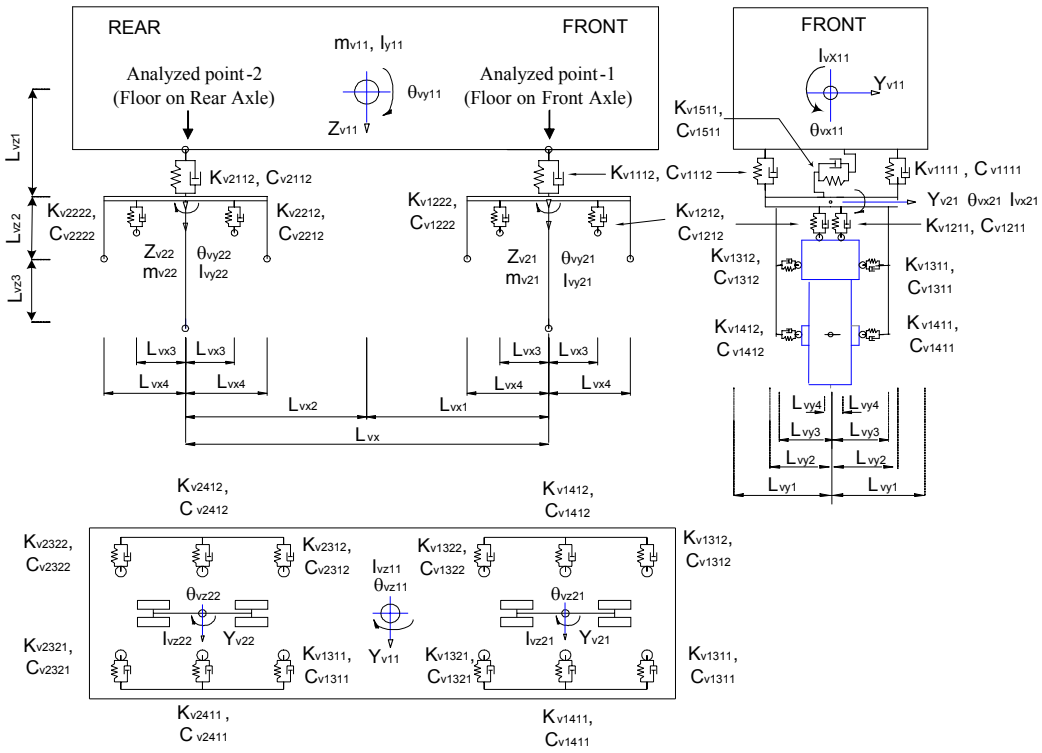

Figure 3. Idealized monorail train with 15DOF

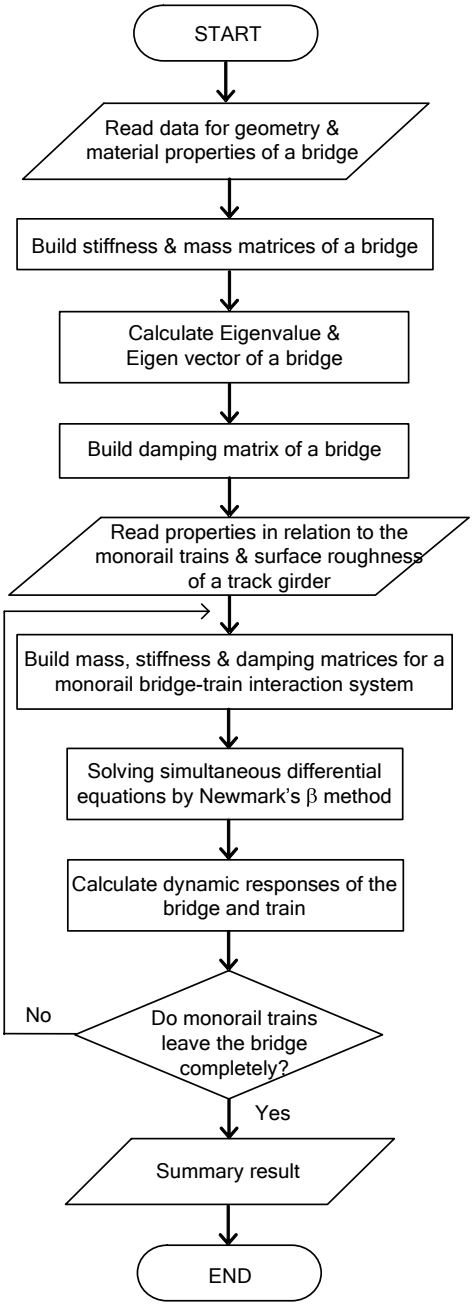

Figure 4. Flowchart to solve the monorail bridge-train interaction problem

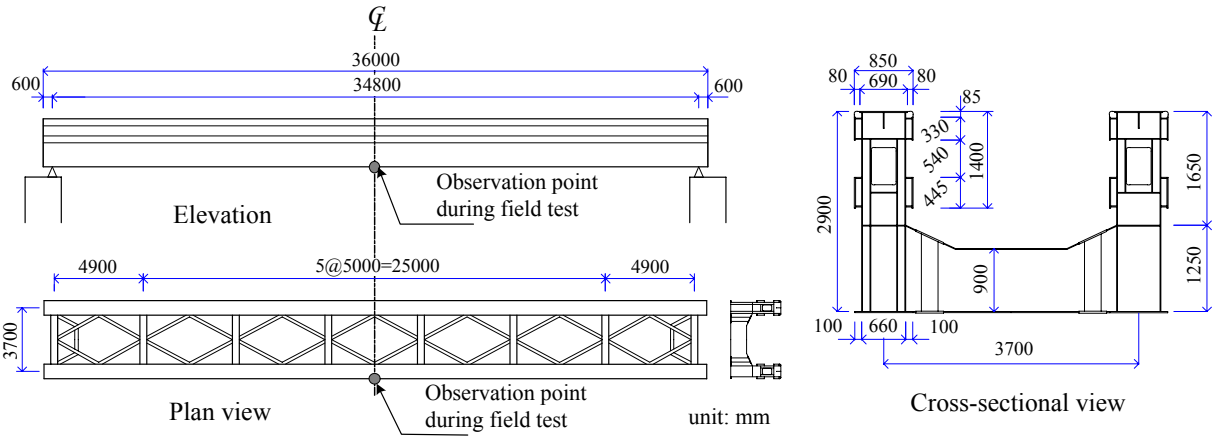

Figure 5. General layout of the monorail bridge tested

a) Video camera equipped with telescope b) Measuring target for displacement

Figure 6. Installation for field-test of monorail bridge

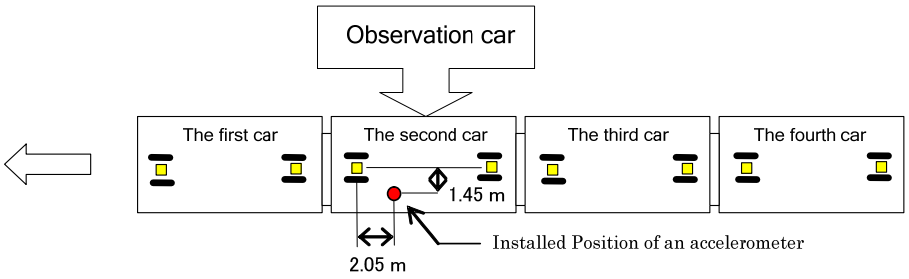

Figure 7. Position of acceleration in a monorail train

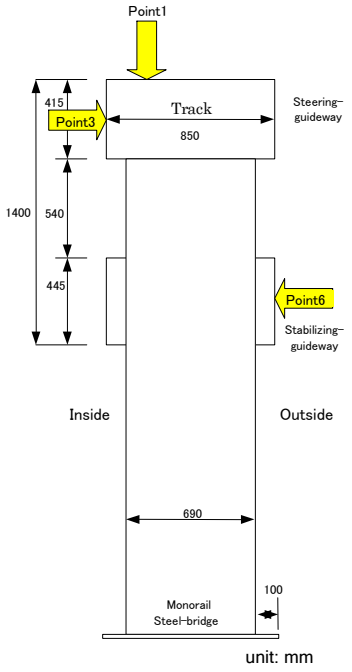

Figure 8. Target position for measuring surface roughness

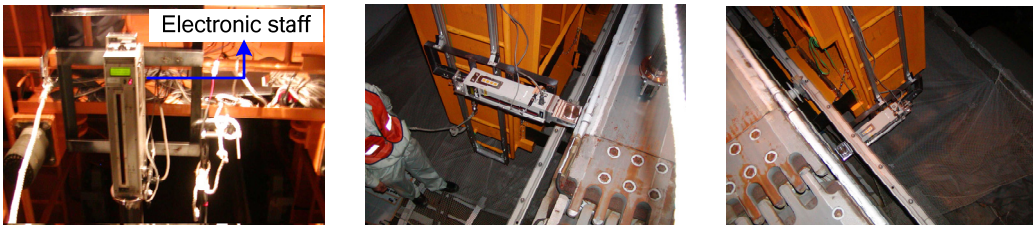

a) Track b) Steering-guideway c) Stabilizing-guideway

Figure 9. Installation of electronic staff to measure surface roughness

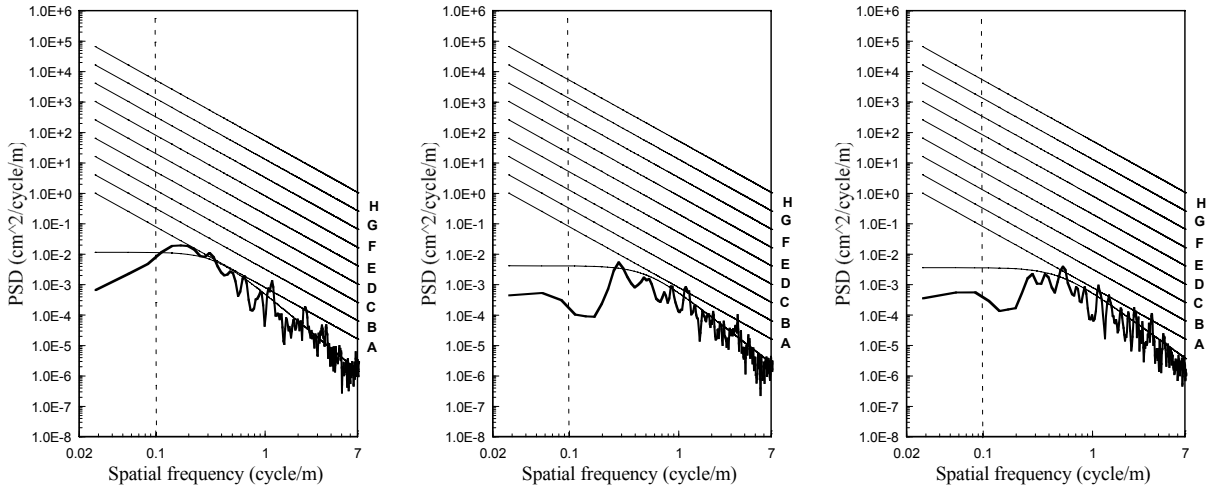

a) Track b) Steering-guideway c) Stabilizing-guideway

Figure 10. PSD curves of measured surface roughness with ISO estimate

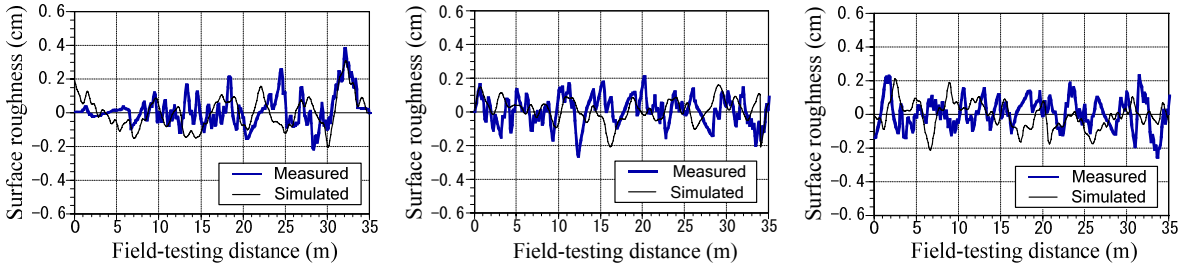

a) Track b) Steering-guideway c) Stabilizing-guideway

Figure 11. Comparison of simulated surface roughness with measured data

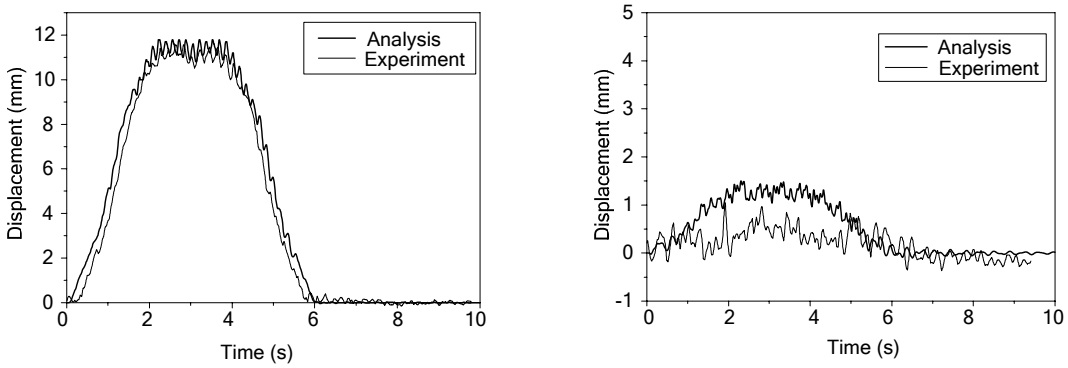

a) Vertical b) Lateral

Figure 12. Analysis vs. Field-test: Displacement of girder

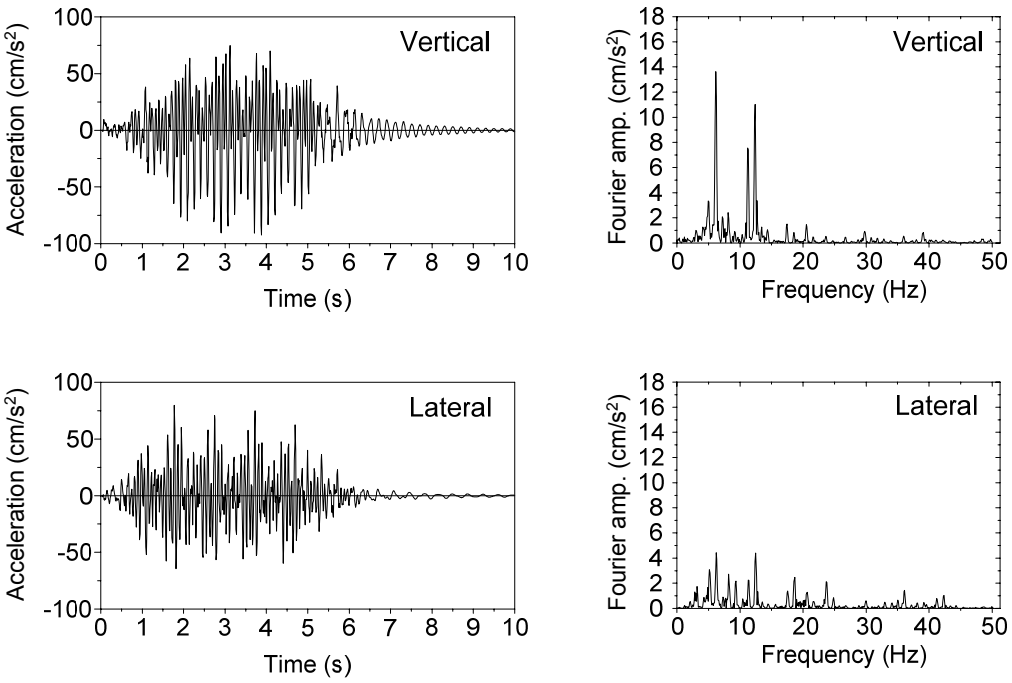

a) Analysis

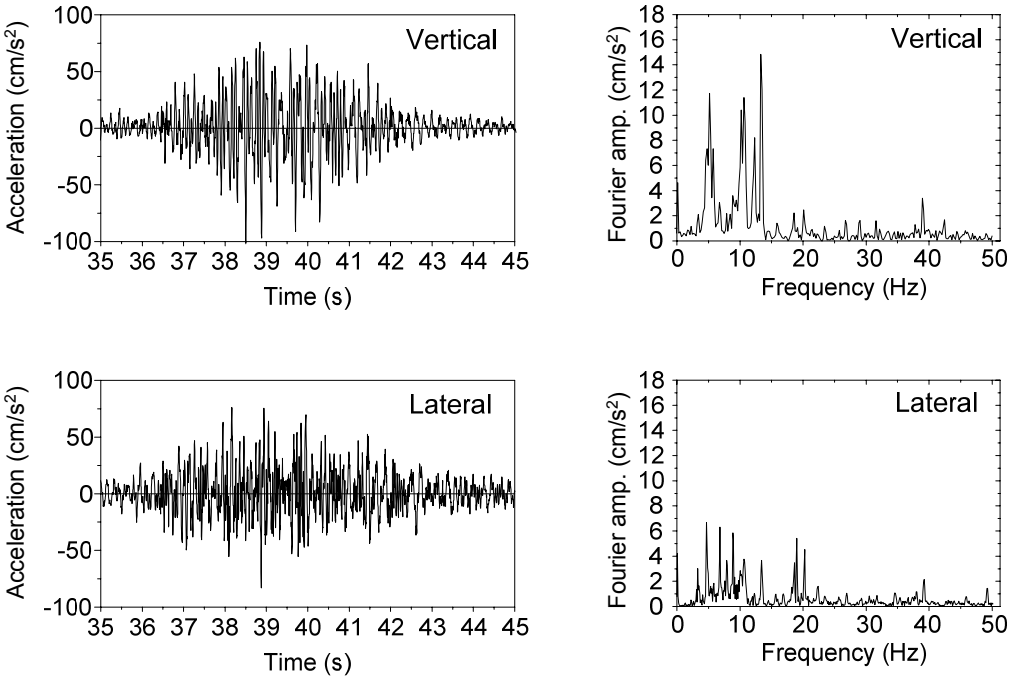

b) Experiment

Figure 13. Analysis vs. Field-test: Acceleration of girder

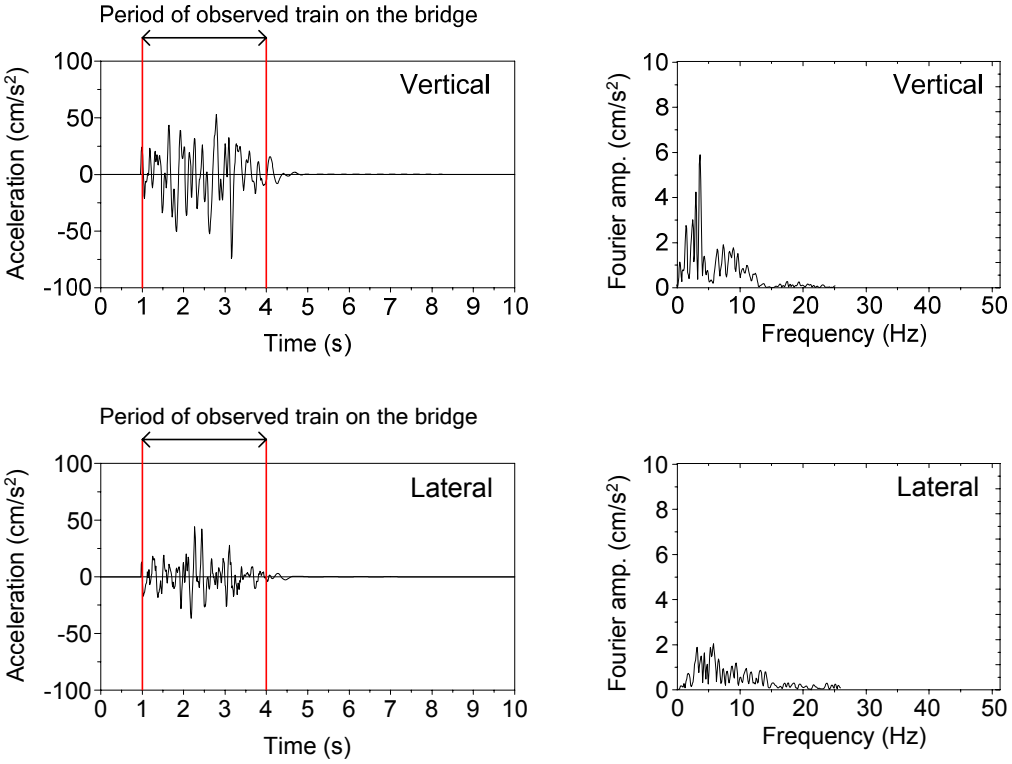

a) Analysis

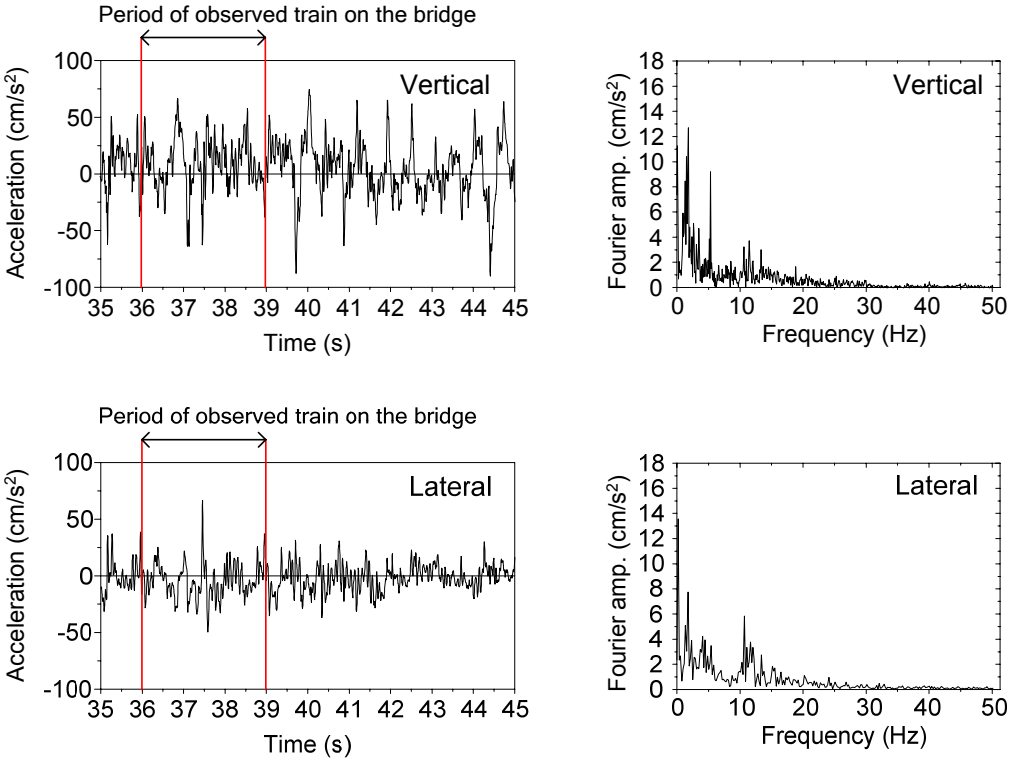

b) Experiment

Figure 14. Analysis vs. Field-test: Acceleration of train

TABLE 1

Notations of train model

Descriptions	Notations
Mass of body	m_{v11}
Mass of suspension system	m_{v21}, m_{v22}
Spring constant of air suspension (vertical)	K_{v1111}, K_{v1112}, K_{v2111}, K_{v2112}
Spring constant of driving wheel	K_{v1211}, K_{v1212}, K_{v1221}, K_{v1222}, K_{v2211}, K_{v2212}, K_{v2221}, K_{v2222}
Spring constant of steering wheel	K_{v1311}, K_{v1312}, K_{v1321}, K_{v1322}, K_{v2311}, K_{v2312}, K_{v2321}, K_{v2322}
Spring constant of stabilizing wheel	K_{v1411}, K_{v1412}, K_{v2411}, K_{v2412}
Spring constant of air suspension (lateral)	K_{v1511}, K_{v2511}
Damping coefficient of air suspension (vertical)	C_{v1111}, C_{v1112}, C_{v2111}, C_{v2112}
Damping coefficient of driving wheel	C_{v1211}, C_{v1212}, C_{v1221}, C_{v1222}, C_{v2211}, C_{v2212}, C_{v2221}, C_{v2222}
Damping coefficient of steering wheel	C_{v1311}, C_{v1312}, C_{v1321}, C_{v1322}, C_{v2311}, C_{v2312}, C_{v2321}, C_{v2322}
Damping coefficient of stabilizing wheel	C_{v1411}, C_{v1412}, C_{v2411}, C_{v2412}
Damping coefficient of air suspension (lateral)	C_{v1511}, C_{v2511}
Vertical and lateral displacements of body	Z_{v11}, Y_{v11}
Vertical displacement of front and rear suspension system	Z_{v21}, Z_{v22}
Lateral displacement of front and rear suspension system	Y_{v21}, Y_{v22}
Rolling, pitching and yawing of body	θ_{vx11}, θ_{vy11}, θ_{vz11}
Rolling of front and rear suspension	θ_{vx21}, θ_{vx22}
Pitching of front and rear suspension system	θ_{vy21}, θ_{vy22}
Yawing of front and rear suspension	θ_{vz21}, θ_{vz22}

TABLE 2

Structural properties of the monorail bridge

Property		Track girder	End cross beam	Cross beam	Lateral bracing
Numbers		2	2	6	28
Young's modulus (GPa)		205	205	205	205
Upper flange	width (mm)	690	300	300	-
	thickness (mm)	18	22	19	-
Web plate	depth (mm)	2782	844	652	176
	thickness (mm)	14	11	9	8
Lower flange	width (mm)	840	300	300	200
	thickness (mm)	(A)*19 (B)*11	22	19	10
Yield stress (MPa)		353	235	235	235

* (A): Thickness at the center of steel box girder, and (B): Thickness at the end of steel box girder.

TABLE 3

Properties of monorail train

Parameter		Notation	Value
Mass (ton)	Body	m_{v11}	14.22
	Bogie	$m_{v21}(=m_{v22})$	6.20
Spring constant (kN/m)	Air suspension (vertical)	$K_{v1111}(=K_{v1112}=K_{v2111}=K_{v2112})$	900.0
	Traveling wheels	$K_{v1211}(=K_{v1212}=K_{v1221}=K_{v1222}=K_{v2211}=K_{v2212}=K_{v2221}=K_{v2222})$	5170.0
	Steering wheels	$K_{v1311}(=K_{v1312}=K_{v1321}=K_{v1322}=K_{v2311}=K_{v2312}=K_{v2321}=K_{v2322})$	6370.0
	Stabilizing wheels	$K_{v1411}(=K_{v1412}=K_{v2411}=K_{v2412})$	6370.0
	Air suspension (lateral)	$K_{v1511}(=K_{v2511})$	980.0
Damping coefficient (kN·s/m)	Air suspension (vertical)	$C_{v1111}(=C_{v1112}=C_{v2111}=C_{v2112})$	22.8
	Traveling wheels	$C_{v1211}(=C_{v1212}=C_{v1221}=C_{v1222}=C_{v2211}=C_{v2212}=C_{v2221}=C_{v2222})$	26.1
	Steering wheels	$C_{v1311}(=C_{v1312}=C_{v1321}=C_{v1322}=C_{v2311}=C_{v2312}=C_{v2321}=C_{v2322})$	185.5
	Stabilizing wheels	$C_{v1411}(=C_{v1412}=C_{v2411}=C_{v2412})$	185.5
	Air suspension (lateral)	$C_{v1511}(=C_{v2511})$	333.6
Geometry (m)		$\lambda_{x1}(=\lambda_{x2})$	4.80
		λ_{x3}	0.75
		λ_{x4}	1.25
		λ_{y1}	1.490
		λ_{y2}	1.025
		λ_{y3}	0.7823
		λ_{y4}	0.2
		λ_{z1}	0.885
		λ_{z2}	0.630
		λ_{z3}	1.715

TABLE 4

Number of passengers during field-test

Experiment case	1st car	2nd car	3rd car	4th car	Total number of passengers	Rate of entrainment
1st	57	40	54	24	175	33.9%
2nd	42	39	34	19	134	25.9%
3rd	35	30	30	21	116	22.5%

TABLE 5

Mode shapes

Mode No.	Mode shape	Natural frequency (Hz)
1	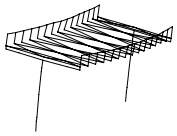	Lateral 1st/T1 (C/W; Pier 1) 2.806 Hz
2	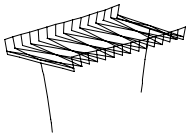	Lateral 1st/T2 (C/W; Pier 2) 2.982 Hz
3	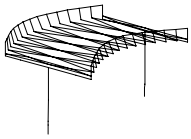	Lateral Bending 1st/T1 5.096 Hz
4	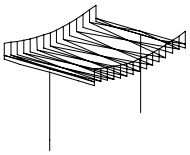	Vertical Bending 1st/T1 5.267 Hz
5	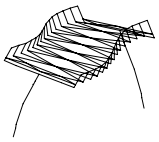	Torsion 1st/T1 (C/W; Pier 2) 8.091 Hz

* C/W: coupled with a pattern of related mode

** T1: both of the track girders have same phase, andT2: both of the track girders have reverse phase

TABLE 6

Natural frequency of train (no passengers loading)

Mode	Natural frequency (Hz)
Bouncing: f_{z11}	1.207
Axle hop (front) : f_{z21}	5.960
Axle hop (Rear) : f_{z22}	5.960
Sway: f_{y11}	0.912
Bogie sway (front) : f_{y21}	4.090
Bogie sway (rear) : f_{y22}	4.090
Rolling: $f_{\theta x11}$	1.660
Axle tramp (front) : $f_{\theta x21}$	4.616
Axle tramp (rear) : $f_{\theta x22}$	4.616
Pitching: $f_{\theta y11}$	1.790
Bogie windup (front): $f_{\theta y21}$	4.394
Bogie windup (rear): $f_{\theta y22}$	4.394
Yawing: $f_{\theta z11}$	2.286
Bogie tramp (front) : $f_{\theta z21}$	4.003
Bogie tramp (rear) : $f_{\theta z22}$	4.003